Heliyon 10 (2024) e29646

Contents lists available at ScienceDirect

Heliyon

journal homepage: www.cell.com/heliyon

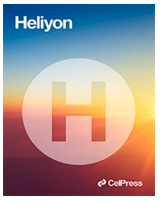

Research article

Production of MgAl/layered double hydroxide microspheres and investigation of the volumetric heat transfer coefficient in spray drying

Luiz D. Silva Neto [a], Lucas Meili [b,*], José T. Freire [a]

[a] Drying Center of Pastes, Suspensions, and Seeds, Department of Chemical Engineering, Federal University of São Carlos (UFSCar), São Carlos, São Paulo, 13565-905, Brazil

[b] Laboratory of Processes, Center of Technology, Federal University of Alagoas, Av. Lourival Melo Mota, s/n, Campus A.C. Simões, Tabuleiro do Martins, Maceió, AL, 57072-970, Brazil

ARTICLE INFO

Keywords:
Layered material
Basal spacing
Heat transfer

ABSTRACT

Layered Double Hydroxides (LDH) are synthetic materials nanostructured in two dimensions that present positively charged layers with interspersed anions for charge and structure balancing. Being recognized as a promising material for various applications, a complete exploration of its possible attractive properties and its synthesis process is essential. However, drying, a necessary step in the process, is still little studied. This work aimed to produce MgAl–CO_3/LDH microspheres and calculate the volumetric heat coefficient in spray drying, evaluating the drying air inlet temperature and the concentration of the feed paste in the dryer. LDH synthesis was carried out using the coprecipitation method, maintaining a 2:1 Mg/Al ratio. The infrared spectra presented the bands characteristic of the hydrotalcite-type material. Through XRD, it was possible to observe that the variation in drying air temperature and feed paste concentration produced LDHs with structural differences. The results obtained for the basal spacing ranged from 7.685 to 7.705 Å. Scanning electron microscopy images confirm the production of LDH microspheres, showing variation in the size of the agglomerates with changes in the feed paste concentration. The volumetric heat transfer coefficient values ranged from 4.31 to 5.36 W m^{-3} K^{-1}, with only the air inlet temperature significantly influencing the process under the conditions studied.

1. Introduction

Layered Double Hydroxides, belonging to a rare and natural group of two-dimensional anionic clays, have been widely studied and used in various fields and strategic areas. Its lamellar structure, porosity, specific surface area, and high ion exchange capacity arouse great interest and present potential uses in the areas of catalysis, biomedical sciences, separation technology, and photochemistry, as a polymer additive, enzyme immobilization, controlled release of pesticides and fertilizers, capture and CO_2 conversion, among others [1–5].

Several synthesis processes were developed and consolidated, compensating for the natural scarcity of LDH and allowing this material's wide range of possibilities, chemical composition, and structural properties. The main synthesis methods are

* Corresponding author. Laboratory of Processes - LAPRO, Technology Center of Federal University of Alagoas, Av. Lourival de Melo Mota, s/n, Campus A. C. Simões, Tabuleiro dos Martins, Maceió, AL, 57072-970, Brazil.
E-mail address: lucas.meili@ctec.ufal.br (L. Meili).

https://doi.org/10.1016/j.heliyon.2024.e29646
Received 18 January 2024; Received in revised form 21 March 2024; Accepted 11 April 2024
Available online 13 April 2024

coprecipitation, hydrothermal synthesis, salt-oxide method, salt-gel method, provoked hydrolysis, ion exchange in solution and in acidic medium, double phase substitutions and regeneration of precursor material [6–14]. Among the synthesis methods, coprecipitation is the most used. It is based on adding a solution containing divalent and trivalent metal cations to a hydroxide solution with the anion to be intercalated. Drying, a necessary step in the process, is still little studied [15,16]. This step directly influences the degradation mechanism of the porous structure, on the agglomeration of particles and evaporation of solvents, being a complex operation and closely linked to the structural arrangement of the material [4,15,17–20].

The appropriate drying method is chosen based on laboratory studies, the characteristics of the raw material, and the product obtained, considering the mechanisms of structural changes, thermal degradation, and shrinkage of the material during the process. Heat and mass transfer mechanisms may vary during drying due to the material's physical structure, temperature, and humidity variations. Usually, oven drying is used to produce LDHs. However, it presents several process limitations [21–24].

Although the basic principles of spray drying may seem simple, it is a complex process regarding mass transfer, heat, and momentum [25,26]. Rotary, jet, fluidized, and atomization dryers have unknown heat and mass transfer interfacial areas, and, for such cases, it is possible to use the volumetric heat and mass transfer coefficient to determine the transfer rate between the media, qualitatively representing the entire volume of the dryer. The spray dryer is one of the industrial dryers that consume the most energy, and its efficiency is strongly linked to the heat transfer between the hot drying air and the atomized droplets. However, few articles in the literature experimentally evaluate the volumetric heat transfer coefficient in spray drying [25–29].

Therefore, this work aims to obtain LDH microspheres through a spray dryer and experimentally evaluate the influence of the drying air inlet temperature and the concentration of the feed paste on the volumetric heat transfer coefficient. The production of microspheres is of interest for applications in heterogeneous catalysis, controlled release of medicines, and adsorption materials, in addition to allowing better handling and safety in an industrial process.

2. Materials and methods

2.1. Synthesis of layered double hydroxide

The syntheses of layered double hydroxides were carried out according to the coprecipitation method described by Reichle [15, 30–33]. A solution of $Mg(NO_3)_2.6H_2O$ and $Al(NO_3)_3.6H_2O$, with a ratio of 2/1, was diluted in deionized water. A secondary solution of 50 % NaOH and anhydrous Na_2CO_3, diluted in deionized water, was added. The reaction was carried out on a mechanical shaker at room temperature. The resulting suspension was kept under stirring at a constant temperature for 18 h. Then, the suspension was centrifuged, and the materials were washed with deionized water at room temperature until they reached pH 10. The colloidal dispersion formed was taken to the drying stage.

2.2. Experimental unit and drying process

The experimental unit used in spray drying was a laboratory-scale spray dryer from Buchi (Mini *Spray Dryer* B-190). The technical specifications of the equipment are found in Table S1. The equipment has a 0.5 mm diameter atomization nozzle with a pneumatic accessory to prevent nozzle clogging.

To evaluate the spray drying process, drying conditions were determined based on available literature and the limitations of the Mini Spray Dryer Büchi 190 [21,23,24]. The effects of drying temperature and paste concentration were investigated. The Spray Dryer inlet temperatures were 175 and 205 °C, and the feed paste concentrations were 3 and 9 %. The compressed air for the atomization and drying airflow were kept constant at 392.27 kPa and 22.5 $m^3\ h^{-1}$, respectively. An external timer and a scale were used to measure the material feed flow. The dilutions were made with deionized water to reach the concentration values and kept under agitation using a magnetic stirrer until the end of the drying process. The temperature and relative humidity of the ambient air were measured using a Tri-Sene® Cole Parmer 37000-90. The dried material was recovered in the cyclone, and the humidity was determined using the oven method, which was maintained at 105 °C for 24 h [34].

2.3. Material characterization

X-ray diffraction analyses were carried out on a Rigaku Multiflex diffractometer, using the powder method, with an incidence of CuKα radiation (λ = 1.5406 Å; 40kV-15mA), 2θ° scanning (2°–90°), speed scanning speed $2\theta°.min^{-1}$ and step 0.02 θ°. Spectroscopy analyses in the Fourier transform infrared (FT-IR) region were carried out using the Shimadzu IRPrestige-21 spectrophotometer in the mid-infrared region in the range of 4000-400 cm-1, using the ATR method with KBr pellets. SEM analyses were carried out using a SHIMADZU scanning electron microscope, model SSX-550 SUPERSACAN, with an acceleration voltage of 20 kV, metallization for 6 min with a gold target at a current of 10 mA.

Basal spacing was calculated according to Pérez-Ramírez et al. (2001) through the Bragg equation (Equation (1)) [35]. The network parameter *a* of the layered structure corresponds to the average distance of the cations within the lamellar layers and can be calculated using Equation (2). The parameter *c*, related to the thickness of the brucite-type lamellar and the interlayer distance, is commonly calculated assuming a 3R polytypism for hydrotalcite (Equation (3)). This calculation is applicable if the d_{00l} reflections are sharp. However, if the reflections are broad, the parameter *c* can be better determined by averaging the position of the diffraction reflections corresponding to the d_{003} and d_{006} value, according to Equation (4) [15].

$$n_r\lambda = 2d_{hkl}.sin\ \theta \quad (1)$$

$$a = 2d_{110} \quad (2)$$

$$c = 3d_{003} \quad (3)$$

$$c = 3(d_{003} + 2d_{006}) / 2 \quad (4)$$

where n_r is the reflection order, λ is the X-ray wavelength used in the analysis, d is the basal spacing for the reflection corresponding to the crystallographic positions of the Miller Indices (hkl), and θ is the determined Bragg angle through the sample peak.

2.4. Calculation of the volumetric heat transfer coefficient (h_V)k

To observe the effects of the drying air inlet temperature (T_{in}) and the LDH concentration in the feed paste (C) on the Volumetric Heat Transfer Coefficient (h_V), a composite experimental design central was adopted from experiments S1 to S4. Thus, 4 axial points and 3 repetitions at the central point were added to obtain a response surface. Table 1 presents the experimental matrix with the variables and levels evaluated, and the *Statistica® 13.0 Statsoft Inc* software was used to obtain the surface.

The volumetric heat transfer coefficient was calculated according to Equation (5) [19,27]:

$$h_V = Q / (V.\Delta T_{log}) \quad (5)$$

where Q is the heat exchanged (kJ.h^{-1}), V is the volume of the spray dryer drying chamber (m^3) and ΔT_{log} is the average logarithmic difference between the inlet and outlet temperatures of the drying chamber. The amount of heat (Equation (6)) is the sum of the amount of heat required for the evaporation of water (Q_{evp}) and the amount of heat required to heat the product ($Q_{heating}$). The amount of heat required to evaporate the water and heat the product was determined using Equations (7) and (8), respectively [27].

$$Q = Q_{evp} + Q_{heating} \quad (6)$$

$$Q_{evp} = W(\lambda + C_{pv}.T_{out} - C_{pw}T_{p1}) \quad (7)$$

$$Q_{heating} = G_{p2}.C_{p2}(T_{p2} - T_{p1}) \quad (8)$$

where W is the amount of water evaporated (kg.h^{-1}), λ is the latent heat of vaporization of water (kJ.kg^{-1}), T_{out} is the exit temperature of the dryer drying chamber (K), T_{p1} is the product inlet temperature (K), C_{pv} is the specific heat of water vapor (kJ.kg^{-1}.K^{-1}), C_{pw} is the specific heat of water (kJ.kg^{-1}.K^{-1}), G_{p2} is the product exit mass flow rate (kg.h^{-1}), C_{p2} is the specific heat of the spray-dried powder (kJ.kg^{-1}.K^{-1}) and T_{p2} is the product exit temperature.

The output mass flow rate of the output product was calculated using Equation (9) [27]:

$$G_{p2} = G_{p1}((1 - w_{p1}) / (1 - w_{p2})) \quad (9)$$

where G_{p1} is the product's input mass flow rate (kg.h^{-1}), w_{p1} and w_{p2} represent the material's humidity on a wet and dry basis, respectively.

The amount of water evaporated is given by Equation (10), and the average logarithmic temperature difference in the drying chamber is determined by Equation (11) [19,36]:

$$W = G_{p1} - G_{p2} \quad (10)$$

Table 1
Experimental planning matrix for spray drying.

Essay	Variable		Coded Variable	
	T_{in} (°C)	C (%)	T_{in} (X_1)	C (X_2)
S1	175	3	−1	−1
S2	175	9	−1	+1
S3	205	3	1	−1
S4	205	9	1	+1
S5	168	6	−1,41	0
S6	211	6	+1,41	0
S7	190	1,8	0	−1,41
S8	190	10,2	0	+1,41
S9	190	6	0	0
S10	190	6	0	0
S11	190	6	0	0

$$\Delta T_{log} = \left(\left(T_{in} - T_{p1}\right) - \left(T_{out} - T_{p2}\right)\right) / \ln\left(\left(T_{in} - T_{p1}\right) / \left(T_{out} - T_{p2}\right)\right) \quad (11)$$

The humidity of the incoming air (X_{in}) is the same as that of the ambient air (X_a). The following equation calculated the ambient air humidity ratio (Equation (12)) and vapor saturation pressure (Equation (13)):

$$X_a = 0,622(P_s.RH) / (P_0 - P_s.RH) \quad (12)$$

$$P_s = exp(46,784 - 6435 / (T_a + 273,15) - 3,868.\ln(T_a + 273,15)) \quad (13)$$

where P_0 is the atmospheric pressure (mmHg), RH is the relative humidity, T_a is the ambient temperature (°C) and P_s is the vapor saturation pressure (mmHg) at a given temperature (Dupré's Equation) [27].

Due to the difficulty of determining the temperature of the particles at the exit of the drying chamber (T_{p2}), we assume that the exit temperature of the particles is equal to the temperature of the saturated surface of the particle, which is represented by the wet bulb temperature (T_w) [25,27]. During spray drying, the droplet of material is heated from its initial temperature, typically room temperature, to the evaporation equilibrium temperature. During this period, moisture removal from the droplet surface follows a constant rate, keeping the droplet at a constant temperature due to the latent heat of vaporization. As the droplet's surface is saturated with moisture, the maximum temperature reached is the wet bulb temperature [25,27]. This way, it means that $T_{p2} = T_w$. The wet bulb temperature can be estimated by Equation (14) [25,37]:

$$T_w = T_{in} - \left((X_{in} - X_{out}).\Delta H_{vap}\right) / C_{p,air} \quad (14)$$

where T_{in} is the air inlet temperature (°C), ΔH_{vap} is the enthalpy of vaporization of water and $C_{p,air}$ is the specific heat of the air.

3. Results and discussion

3.1. X-ray diffraction

For the LDHs produced, XRD analyses were carried out for all drying temperature conditions. A typical XRD pattern for LDH is shown in Fig. 1. Characteristic reflections similar to hydrotalcite-type materials with 2θ = 11.56° (003), 23.20° (006), 34.70° (009/012), 46.52° (018), 60.76° (110) and 62.22° (113) were displayed, proving the synthesis of the material (Fig. 1a). The basal planes (00*l*) indicate the degree of crystal growth, while the non-basal planes (0 *kl*) suggest faults in the structure's stacking [38]. The peak at 2θ = 29° is related to sodium nitrate [39–41]. The change in spray drying parameters influenced the intensity and width of reflections (Fig. 1b), providing low crystalline phase and stacking defects. The diffractograms of MgAl–CO_3/LDH obtained by oven drying generally present clear and symmetrical reflections, illustrating a well-defined and crystalline structure [42]. Some studies that used freeze-drying as a drying method also showed broader reflections with lower intensity in the diffractograms of the LDHs produced [20,43–45].

The results obtained by diffraction made it possible to determine the basal spacings, lattice parameters, and the average size of the crystallites [15,43]. The basal spacing (d_{003} value) and the parameters *a* and *c*, referring to the distance between the metal ions in the lamellar layer and the lamellar stacking, respectively, are shown in Table 2. The results demonstrate that the variation in drying parameters produced LDHs with structural differences. The results obtained for the d_{003} value range from 7.685 to 7.705 Å. Since the parameter *c* is directly related to the d_{003} value, this result suggests an influence on the stacking and degree of hydration in these materials [43]. Fig. 2 shows the variation in basal spacing as a function of temperature and paste concentration. Assessing the effect of temperature (Fig. 2a), it is possible to observe that the 9 % paste concentration increased basal spacing with increasing temperature. The 3 % paste concentration showed the opposite behavior, decreasing with increasing temperature. By keeping the temperature constant and increasing the paste concentration (Fig. 2b), there was an increase in the basal spacing for both concentrations, showing a

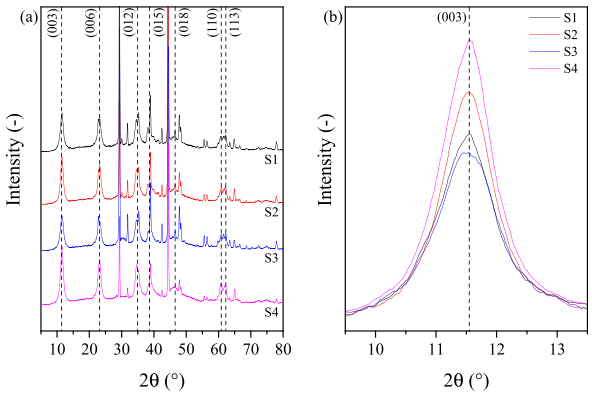

Fig. 1. Diffractogram of the LDHs obtained from spray drying: (a) reflections characteristics for LDH; (b) diffractogram of the (003) plane.

Table 2
Basal spacing and network parameter of spray dried LDHs.

Sample	Basal spacing (Å)		Lattice Parameters (Å)	
	d_{003}	d_{110}	a	c
S1 (175 °C/3 %)	7705	1,52	3,05	23,163
S2 (175 °C/9 %)	7685	1,52	3,05	23,062
S3 (205 °C/3 %)	7694	1,52	3,05	23,168
S4 (205 °C/9 %)	7691	1,52	3,05	23,144

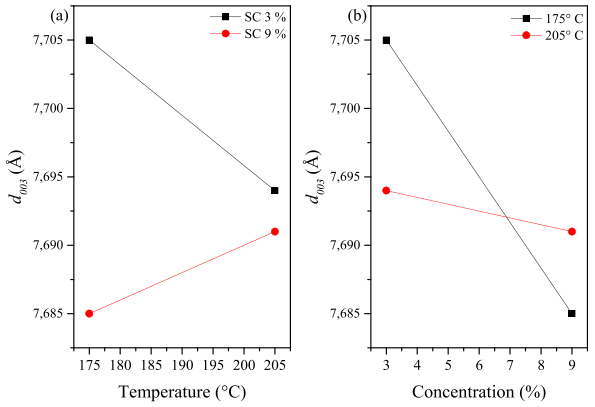

Fig. 2. Basal spacing: (a) variation as a function of drying air inlet temperature; (b) variation as a function of feed paste concentration.

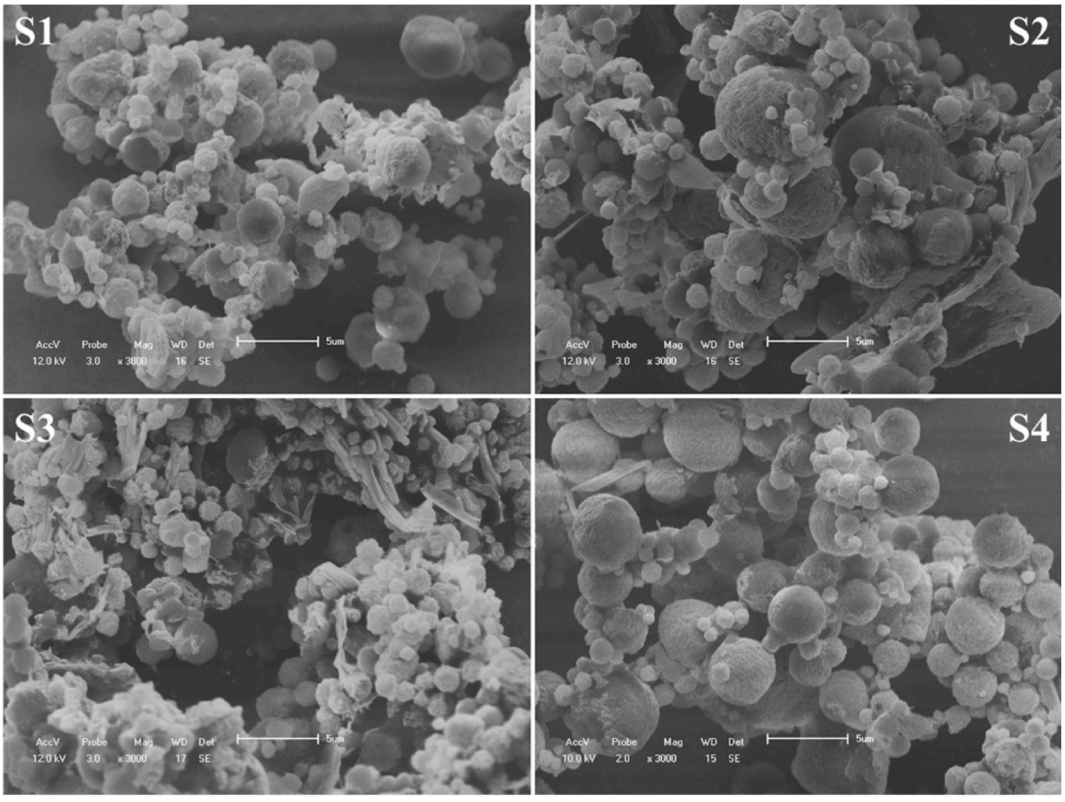

Fig. 3. Representative scanning electron microscopy images of atomized LDHs obtained with different drying conditions: S1 (175 °C/3 %); S2 (175 °C/9 %); S3 (205 °C/3 %); S4 (205 °C/9 %).

more pronounced behavior at a temperature of 175 °C. In addition to directly impacting the basal spacing of the layered double hydroxide, this result directly impacts the average size of the crystallites, especially in mathematical equations that heavily depend on this plane for the calculation, such as the Scherrer equation. Yang et al. (2002) presents the structural evolution of MgAl–CO_3/LDH in the calcination process, where there is a decrease in the basal spacing and in the parameter c when the material leaves the temperature of 70 °C and reaches 190 °C [46]. Silva Neto et al. (2021) shows a decrease in basal spacing with an increase in drying temperature from 75 °C to 105 °C, showing a decrease in spacing due to the removal of interlayer water resulting from the increase in drying temperature [15]. Given this, some other drying parameters may influence basal spacing more than temperature, and an isolated study of these parameters is necessary.

As all LDHs produced have the same metallic cations in the lamellar layers (magnesium and aluminum), the ionic radius between them remains constant, and the lattice parameter a does not undergo significant changes in its value [47,48].

3.2. Scanning electron microscopy

Fig. 3 presents the images obtained through scanning electron microscopy for the different essay, showing the morphology of the materials obtained. The images confirm the production of LDH microspheres without using any binder in all experimental conditions evaluated. The materials presented a spherical shape, smooth surface and no holes.

The characteristics of the feed paste are very important for the spray drying process. The size of the dry agglomerates is mainly determined by the size of the droplets generated in the atomizer. Fig. 3 shows that the drying parameters studied influenced the size of the MgAl–CO_3/LDH microspheres. Increasing the concentration of LDH in the feed paste from 3 % to 9 % increased the size of the agglomerates at the two temperatures studied (Fig. 3 S2 and S4). The size of the droplets generated by the atomizer varies with the viscosity of the feed paste at the same atomization rate [49,50]. Thus, the effect of increasing concentration causes an increase in the viscosity of the paste, dampening energy oscillations on the surface of the liquid and generating the formation of larger droplets in the atomization process. The lower viscosity of the paste at 3 % concentration provides better atomization of the material and, consequently, a greater quantity of particles and less agglomeration (Fig. 3 S1 and S3) [22,51]. This behavior was also observed by Julklang et al. (2017) in the manufacture of LDH microspheres by spray drying, with larger average sizes of LDH agglomerates from higher paste concentrations. Evaluating the influence of maltodextrin concentration on the yield of açaí pulp microencapsulation by atomization, Tonon et al. (2008) observed that increasing the concentration of maltodextrin increased the viscosity of the feed paste, generating larger agglomerates of particles at the end of the process and reducing the powder yield [52].

Increasing the drying air temperature causes an increase in the rate of water evaporation, resulting in larger particles due to less time for shrinkage and the accelerated formation of these microspheres. Julklang et al. (2017) suggest that the average size of LDH clusters increases slightly with increasing drying air temperature due to the increased evaporation rate of droplets in the drying chamber [21]. Similar trends were observed by Nijdam and Langrish (2006), Tonon et al. (2008), and Shishir et al. (2016), obtaining smaller particles with lower drying air temperatures in the atomization process [52–54]. This behavior could not be confirmed for this work through scanning electron microscopy alone.

The morphology resulting from the calcination of LDH microspheres was observed by Wang et al. (2008) and Shi et al. (2015). The authors found that the layered double oxide from calcination maintained the shape of microspheres, making the spray drying process interesting for obtaining these microspheres [23,24].

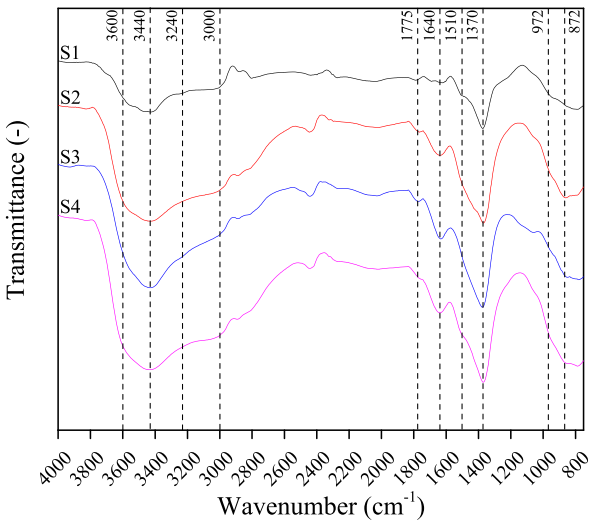

Fig. 4. Spectrum of the infrared region of the layered double hydroxide.

3.3. Fourier transform infrared spectroscopy

Through the results of the spectra in the infrared region, three general types of vibrations can be found in LDHs: molecular vibrations of the hydroxyl groups, lattice vibrations of the octahedral sheets of the material, and vibrations of the intercalated anions. The spectra of the infrared region of MgAl–CO_3/LDH obtained through spray drying are represented in Fig. 4. All LDHs produced and characterized by FTIR showed the characteristic bands of the hydrotalcite-type material [42].

As shown in Fig. 4, all spectra showed a broad band between 3900 and 2500 cm^{-1}, which exhibits vibrations related to hydroxyl stretching from the lamellar layer and water molecules. These hydroxyl-water stretching vibrations are intense in the infrared due to the change in dipole moment. The amplitude of these bands indicates that the chemical bonds of these vibrations are of the hydrogen bond type [55]. The bands present in the 3690-3500 cm-1 region are attributed to the vibration of the Mg–Al–OH bond in LDH or in $Mg_2Al(OH)_7$ [55]. In the region 3500-3300 cm^{-1}, superimposed OH vibrations are attributed, possibly originating from the metal in the lamellar layer, giving interlayer water and solvated carbonate [56]. The vibration bands around 3440 cm^{-1} and 3030 cm^{-1} can be attributed to stretching the O–H bond of hydroxyl groups, interspersed water molecules, and physically adsorbed water. The 3000 cm^{-1} band is related to the hydrogen bonding of H_2O to CO_3^{2-} ions in the interlayer space. Although generally not mentioned, the 1775 cm^{-1} band is also attributed to interlayer water vibrations, showing the same decreasing behavior as the characteristic band around 3000 cm^{-1} in IR spectra with increasing temperature. The 1640 cm^{-1} band is mainly due to the H–*O*–H bending of physically adsorbed water [15,35,55,57].

The carbonate ion (CO_3^{2-}) is a nonlinear atomic species with the geometry of a flat triangle with four atoms and belongs to the D_{3h} point group. Thus, the ion can be found in more than one atomic species in the interlayer layer of LDHs. The band around 1510 cm^{-1} is attributed to the vibrations of the symmetry reduced to monodentate carbonates, which interact with the metal of the lamellar layer. Furthermore, the spectra indicate that bidentate carbonate bands are formed at 1370 cm^{-1} [44,47]. According to some authors, bands around 1440 cm^{-1} are also attributed to vibrations of CO_3^{2-} groups, suggesting a lower symmetry of carbonate groups, characteristic of free ions, relatively undistorted and possibly present on the surface [58–62].

The bands between 800 and 400 cm^{-1} may be due to the superposition of vibrational absorptions of magnesium and aluminum oxides [61,63]. Carbonate stability is no longer determined by the hydrotalcite structure but by interactions with metal ions in the mixed oxide phase, leading to the observed trend. The bands around 972 and 872 cm^{-1} can be derived from the stretching of O–H and the deformation of the metal-OH bonds, separated from the octahedral sheets [35].

3.4. Volumetric heat transfer coefficient (h_V)k

Table 3 presents the experimental results for spray drying. The values for h_V for the Mini Spray Dryer Büchi 190, under the conditions studied, it ranged from 4.31 to 5.36 W m^{-3} K^{-1}, coinciding with the results found by Lisboa et al. (2018) [25]. However, compared to some spray drying works, the volumetric heat transfer coefficient obtained in this work was lower [10,18,19]. According to Mujumdar et al. (2014), classic spray dryers have a volumetric heat transfer coefficient of around 130–180 W m^{-3} K^{-1} [19,27].

This low value of h_V may be due to the low mass flow rate of the material used in this work. Equation (7) shows that Q_{evp} is directly proportional to the amount of water evaporated, in kg.h^{-1}. Nguyen et al. (2020) used an inlet mass flow rate of around 20 kg h^{-1} for soy milk. This work used an inlet mass flow rate of 0.45 kg h^{-1}, 40 times lower than the flow rate in their work [27]. Rajasekar and Raja (2023) investigated the heat and mass transfer characteristics during the synthesis of the $Na_2Fe_{0.6}Mn_{0.4}PO_4F/C$ catalyst through intermittent spray drying with an inlet mass flow rate varying between 3.50 and 6.95 kg h^{-1}, obtaining values between 1.5 e 3.5 W m^{-3} K^{-1} for the volumetric heat transfer coefficient [28].

The effect of the drying air inlet temperature and the LDH concentration in the feed paste on the volumetric heat transfer coefficient in spray drying of MgAl–CO_3/LDH is presented in Fig. 5. Fig. 5a shows the behavior of h_V with the variation of the evaluated parameters, indicating a significant influence of the air inlet temperature. The Pareto chart (Fig. 5b) shows that only the Temperature variable had a significant influence on h_V, as observed on the response surface.

Fig. 6a shows that the volumetric heat transfer coefficient decreased with the increase in inlet air temperature. The highest and lowest h_V values found were 5.36 and 4.31 W m^{-3} K^{-1} precisely at the axial points with the lowest and highest temperatures, 168 and

Table 3
Experimental results for calculating the volumetric heat transfer coefficient.

Essay	T_{in} (°C)	C (%)	T_{out} (°C)	T_w (°C)	ΔT_{log} (–)	h_V (W.m^{-3}.K^{-1})
S1	175	3	101	82.15	62.96	4.81
S2	175	9	109	89.68	64.33	4.74
S3	205	3	135	117.81	68.79	4.54
S4	205	9	135	117.18	69.60	4.45
S5	168	6	108	93.18	56.76	5.36
S6	211	6	135	116.82	72.73	4.31
S7	190	1,8	121	105.95	62.63	4.94
S8	190	10,2	113	98.47	61.67	4.92
S9	190	6	113	99.49	60.28	5.06
S10	190	6	113	97.65	62.49	4.87
S11	190	6	113	99.54	59.97	5.08

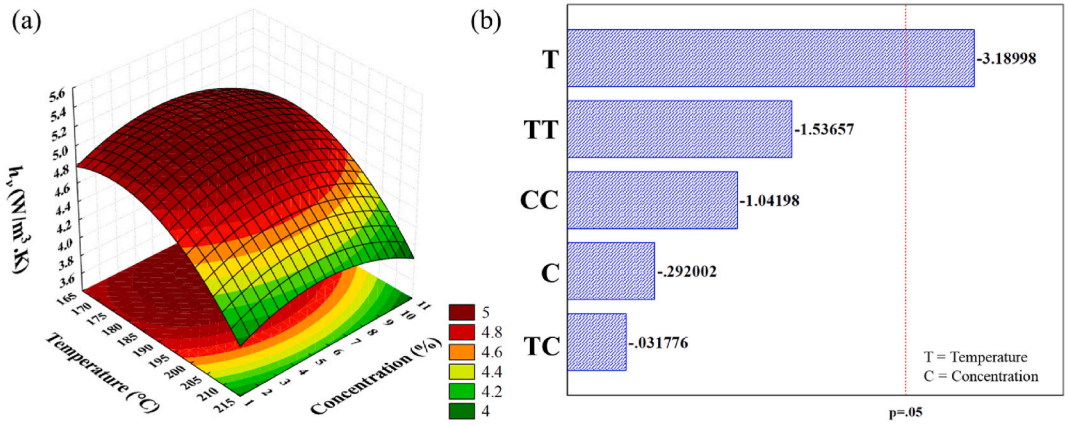

Fig. 5. Effect of inlet air temperature and feed paste concentration on the volumetric heat transfer coefficient: (a) response surface; (b) pareto chart.

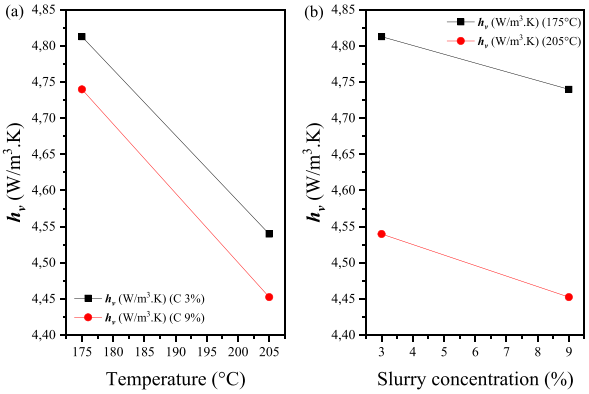

Fig. 6. Volumetric heat transfer coefficient: (a) variation as a function of drying air inlet temperature; (b) variation as a function of feed paste concentration.

211 °C, respectively. The increase in air temperature at the inlet caused a greater difference between the inlet and outlet temperatures in the equipment and, with h_V being inversely influenced by ΔT_{log}, as can be seen in Equation 5.3, this result is consistent. Furthermore, the increase in the inlet air temperature possibly causes a decrease in the average residence time of the particles due to the reduction in air density, increasing speed and drag of the particles in the drying process. This behavior can be observed in Table 3, essay 3 and 4 presented higher values of ΔT_{log} and lower values of reduction of T_w (in percentage) about essay S1 and S2, where the drying temperature is smaller. According to Lisboa et al. (2018), the wet bulb temperature is about 12 % below the outlet temperature, and this was observed in experiments S3 and S4, but for essay S1 and S2, this percentage reaches around 18 % [25]. According to the Pareto chart (Fig. 5b), the feed concentration had no significant effect on the volumetric heat transfer coefficient. However, Nguyen et al. (2020) reported that the increase in the amount of solids in the atomized droplets due to the increase in concentration implies a decrease in the amount of water evaporated in the drying chamber [27]. Thus, the total amount of heat the particles receive decreases, consequently decreasing the volumetric heat transfer coefficient. This behavior was also present in the main points (essay S1 to S4) of the planning studied in this work (Fig. 6b), with the h_V decreasing with the increase in MgAl–CO_3/LDH concentration.

4. Conclusion

The layered double hydroxides MgAl–CO_3/LDH were obtained through spray drying under all studied conditions. XRD, SEM, and FTIR analyses confirmed the synthesis and formation of LDH microspheres without adding any dispersant or binder. The results showed that changes in the drying air inlet temperature and the paste concentration in the dryer feed caused morphological variations in the LDHs, presenting differences in the basal spacing, in the network parameter *c*, and in the size of the agglomerates. Furthermore, the change in drying air temperature caused a variation in the volumetric heat transfer coefficient, between 4.310 e 5.360 W m^{-3} K^{-1}. The h_V is used to quantify heat transfer since the exact specific surface area of active heat transfer between the drying medium and the LDH droplets is unknown. Therefore, work on optimizing the production of LDH microspheres by spray drying must consider the basal spacing, porosity, particle size, and agglomeration, among other particularities of this material.

Funding

This work was supported by the Conselho Nacional de Desenvolvimento Científico e Tecnológico (CNPq/Brazil), Coordenação de Aperfeiçoamento de Pessoal de Nível Superior (CAPES/Brazil).

CRediT authorship contribution statement

Luiz D. Silva Neto: Writing – review & editing, Writing – original draft, Visualization, Methodology, Investigation, Formal analysis, Data curation, Conceptualization. **Lucas Meili:** Writing – review & editing, Supervision, Resources, Funding acquisition, Conceptualization, Writing – original draft. **José T. Freire:** Writing – review & editing, Writing – original draft, Supervision, Resources, Conceptualization.

Declaration of competing interest

The authors declare the following financial interests/personal relationships which may be considered as potential competing interests:I am an associated editor of Heliyon – Chemical Engineering section.

Appendix A. Supplementary data

Supplementary data to this article can be found online at https://doi.org/10.1016/j.heliyon.2024.e29646.

References

[1] L. guo L.-G. Yan, K. Yang, R.-R. Shan, T. Yan, J. Wei, S.-J.S. jun Yu, H.-Q.H. qin Yu, B. Du, Kinetic, isotherm and thermodynamic investigations of phosphate adsorption onto core-shell Fe3O4@LDHs composites with easy magnetic separation assistance, J. Colloid Interface Sci. 448 (2015) 508–516, https://doi.org/10.1016/j.jcis.2015.02.048.

[2] K. Abdellaoui, I. Pavlovic, M. Bouhent, A. Benhamou, C. Barriga, A comparative study of the amaranth azo dye adsorption/desorption from aqueous solutions by layered double hydroxides, Appl. Clay Sci. 143 (2017) 142–150, https://doi.org/10.1016/j.clay.2017.03.019.

[3] L. Meili, P.V. Lins, C.L.P.S. Zanta, J.I. Soletti, L.M.O. Ribeiro, C.B. Dornelas, T.L. Silva, M.G.A. Vieira, MgAl-LDH/Biochar composites for methylene blue removal by adsorption, Appl. Clay Sci. 168 (2019) 11–20, https://doi.org/10.1016/j.clay.2018.10.012.

[4] C. Dazon, C. Taviot-Guého, V. Prévot, Layered double hydroxides: where should research stress on for massive scaling up? Mater. Adv. 4 (2023) 4637–4645, https://doi.org/10.1039/d3ma00478c.

[5] S. Mallakpour, M. Hatami, C.M. Hussain, Recent innovations in functionalized layered double hydroxides: fabrication, characterization, and industrial applications, Adv. Colloid Interface Sci. 283 (2020) 102216, https://doi.org/10.1016/j.cis.2020.102216.

[6] Y.D.G. Edañol, J.A.O. Poblador, T.J.E. Talusan, L.M. Payawan, Co-precipitation synthesis of Mg-Al-CO3layered double hydroxides and its adsorption kinetics with phosphate(V) ions, Mater. Today Proc. 33 (2020) 1809–1813, https://doi.org/10.1016/j.matpr.2020.05.059.

[7] T. Hibino, H. Ohya, Synthesis of crystalline layered double hydroxides: precipitation by using urea hydrolysis and subsequent hydrothermal reactions in aqueous solutions, Appl. Clay Sci. 45 (2009) 123–132, https://doi.org/10.1016/j.clay.2009.04.013.

[8] G. Rathee, A. Awasthi, D. Sood, R. Tomar, V. Tomar, R. Chandra, A new biocompatible ternary Layered Double Hydroxide Adsorbent for ultrafast removal of anionic organic dyes, Sci. Rep. 9 (2019) 1–14, https://doi.org/10.1038/s41598-019-52849-4.

[9] D. Sokol, D.E.L. Vieira, A. Zarkov, M.G.S. Ferreira, A. Beganskiene, V.V. Rubanik, A.D. Shilin, A. Kareiva, A.N. Salak, Sonication accelerated formation of Mg-Al-phosphate layered double hydroxide via sol-gel prepared mixed metal oxides, Sci. Rep. 9 (2019) 1–9, https://doi.org/10.1038/s41598-019-46910-5.

[10] K.H. Goh, T.T. Lim, Z. Dong, Application of layered double hydroxides for removal of oxyanions: a review, Water Res. 42 (2008) 1343–1368, https://doi.org/10.1016/j.watres.2007.10.043.

[11] N. Iyi, T. Matsumoto, Y. Kaneko, K. Kitamura, Deintercalation of carbonate ions from a hydrotalcite-like compound: enhanced decarbonation using acid-salt mixed solution, Chem. Mater. 16 (2004) 2926–2932, https://doi.org/10.1021/cm049579g.

[12] L. Palin, C. Lamberti, Å. Kvick, F. Testa, R. Aiello, M. Milanesio, D. Viterbo, Single-crystal synchrotron radiation X-ray diffraction study of B and Ga silicalites compared to a purely siliceous MFI: a discussion of the heteroatom distribution, J. Phys. Chem. B 107 (2003) 4034–4042, https://doi.org/10.1021/jp027586r.

[13] S.V. Prasanna, P.V. Kamath, Anion-exchange reactions of layered double hydroxides: interplay between coulombic and h-bonding interactions, Ind. Eng. Chem. Res. 48 (2009) 6315–6320, https://doi.org/10.1021/ie9004332.

[14] D.Y. Wang, F.R. Costa, A. Vyalikh, A. Leuteritz, U. Scheler, D. Jehnichen, U. Wagenknecht, L. Ḧaussler, G. Heinrich, One-step synthesis of organic LDH and its comparison with regeneration and anion exchange method, Chem. Mater. 21 (2009) 4490–4497, https://doi.org/10.1021/cm901238a.

[15] L.D. Silva Neto, C.G. Anchieta, J.L.S. Duarte, L. Meili, J.T. Freire, Effect of drying on the fabrication of MgAl layered double hydroxides, ACS Omega 6 (2021) 21819–21829, https://doi.org/10.1021/acsomega.1c03581.

[16] M.V. Bukhtiyarova, A review on effect of synthesis conditions on the formation of layered double hydroxides, J. Solid State Chem. 269 (2019) 494–506, https://doi.org/10.1016/j.jssc.2018.10.018.

[17] B.H. Wang, C.Y. Yu, X.Z. Wang, Supercritical drying for nanometer porous materials, in: Proc. Eighth Natl. Dry. Symp., Harbin, 2002, pp. 22–31.

[18] W. Zhang, B. Wang, F. Fan, W. Zhang, A.S. Mujumdar, L. Huang, Effect of different drying methods on the morphology and particle size of magnesium oxide nanoparticles, in: Int. Work. Symp. Ind. Dry., 2004, pp. 427–432. Mumbai.

[19] A.S. Mujumdar, Handbook of Industrial Drying, fourth ed., CRC Press, 2014.

[20] S. Moriyama, K. Sasaki, T. Hirajima, Effect of freeze drying on characteristics of Mg–Al layered double hydroxides and bimetallic oxide synthesis and implications for fluoride sorption, Appl. Clay Sci. 132–133 (2016) 460–467, https://doi.org/10.1016/j.clay.2016.07.016.

[21] W. Julklang, A. Wangriya, B. Golman, Fabrication of layered double hydroxide microspheres by spray drying of nanoparticles: effects of process conditions, Mater. Lett. 209 (2017) 429–432, https://doi.org/10.1016/j.matlet.2017.08.067.

[22] W. Julklang, B. Golman, Numerical simulation of spray drying of hydroxyapatite nanoparticles, Clean Technol. Environ. Policy 17 (2015) 1217–1226, https://doi.org/10.1007/s10098-015-0931-z.

[23] J. Le Shi, H.J. Peng, L. Zhu, W. Zhu, Q. Zhang, Template growth of porous graphene microspheres on layered double oxide catalysts and their applications in lithium-sulfur batteries, Carbon N. Y. 92 (2015) 96–105, https://doi.org/10.1016/j.carbon.2015.03.031.

[24] Y. Wang, T. Zhang, S. Xu, X. Wang, D.G. Evans, X. Duan, Preparation of layered-double hydroxide microspheres by spray drying, Ind. Eng. Chem. Res. 47 (2008) 5746–5750, https://doi.org/10.1021/ie800146m.

[25] H.M. Lisboa, M.E. Duarte, M.E. Cavalcanti-Mata, Modeling of food drying processes in industrial spray dryers, Food Bioprod. Process. 107 (2018) 49–60, https://doi.org/10.1016/j.fbp.2017.09.006.

[26] P. Van Khanh, T.T.T. Hang, Evaluation of heat and mass transfer efficiency of milk spray drying by computational simulation tool, J. Mech. Eng. Res. Dev. 44 (2021) 251–259.

[27] D.Q. Nguyen, T.H. Nguyen, K. Allaf, Volumetric heat transfer coefficient in spray drying of soymilk powder, Dry. Technol. 40 (2020) 1146–1152, https://doi.org/10.1080/07373937.2020.1857768.

[28] K. Rajasekar, B. Raja, Heat and mass transfer characteristics during spray drying of Na2Fe0.6Mn0.4PO4F/C cathode material for Na-ion batteries, Appl. Therm. Eng. 221 (2023) 119838, https://doi.org/10.1016/j.applthermaleng.2022.119838.

[29] K. Rajasekar, B. Raja, An investigation on heat and mass transfer characteristics during spray drying of saline water, Sadhana - Acad. Proc. Eng. Sci. 47 (2022) 1–17, https://doi.org/10.1007/s12046-022-01863-w.

[30] W.T. Reichle, Synthesis of anionic clay minerals (mixed metal hidroxides, hydrotalcite), Solid State Ionics 22 (1986) 135–141.

[31] W.T. Reichle, Catalytic reactions by thermally activated , synthetic , anionic clay minerals, J. Catal. 94 (1985) 547–557.

[32] A.P. Tathod, N. Hayek, D. Shpasser, D.S.A. Simakov, O.M. Gazit, Mediating interaction strength between nickel and zirconia using a mixed oxide nanosheets interlayer for methane dry reforming, Appl. Catal. B Environ. 249 (2019) 106–115, https://doi.org/10.1016/j.apcatb.2019.02.040.

[33] G.E. Santos, A.H. Ide, J.L.S. Duarte, G. McKay, A.O.S. Silva, L. Meili, Adsorption of anti-inflammatory drug diclofenac by MgAl/layered double hydroxide supported on Syagrus coronata biochar, Powder Technol. 364 (2020) 229–240, https://doi.org/10.1016/j.powtec.2020.01.083.

[34] F.J. Gómez-De La Cruz, F. Cruz-Peragón, P.J. Casanova-Peláez, J.M. Palomar-Carnicero, A vital stage in the large-scale production of biofuels from spent coffee grounds: the drying kinetics, Fuel Process. Technol. 130 (2015) 188–196, https://doi.org/10.1016/j.fuproc.2014.10.012.

[35] J. Pérez-Ramírez, G. Mul, F. Kapteijn, J.A. Moulijn, A spectroscopic study of the effect of the trivalent cation on the thermal decomposition behaviour of Co-based hydrotalcites, J. Mater. Chem. 11 (2001) 2529–2536, https://doi.org/10.1039/b104989p.

[36] I. Filková, A.S. Mujumdar, Industrial spray drying systems, 2., in: A.S. Mujumdar (Ed.), Handb. Ind. Dry, Marcel Dekker, USA, 1995, pp. 263–308.

[37] W.L. McCabe, J.C. Smith, P. Harriot, Unit Operations of Chemical Engineering, fifth ed., McGraw-Hill, Inc., New York, 1993.

[38] A.V. Radha, P.V. Kamath, C. Shivakumara, Conservation of order, disorder, and "crystallinity" during anion-exchange reactions among Layered Double Hydroxides (LDHs) of Zn with Al, J. Phys. Chem. B 111 (2007) 3411–3418, https://doi.org/10.1021/jp0684170.

[39] C. Wang, Y. Li, G. You, Q. Zhu, The promotional effect of sodium chloride on thermophysical properties of nitrate, IOP Conf. Ser. Mater. Sci. Eng. 772 (2020) 012033, https://doi.org/10.1088/1757-899X/772/1/012033.

[40] S. Miao, Z. Luo, S. Tan, T. Xu, Z. Zhou, G. Feng, G. Xu, G. Ji, Mg-Al layered double hydroxides film coating for efficient biomimetic stealth, Prog. Org. Coating 186 (2024) 108074, https://doi.org/10.1016/j.porgcoat.2023.108074.

[41] K. Shekoohi, F.S. Hosseini, A.H. Haghighi, A. Sahrayian, Synthesis of some Mg/Co-Al type nano hydrotalcites and characterization, MethodsX 4 (2017) 86–94, https://doi.org/10.1016/j.mex.2017.01.003.

[42] A.F. da Silva, J.L. da S. Duarte, L. Meili, Different routes for MgFe/LDH synthesis and application to remove pollutants of emerging concern, Sep. Purif. Technol. 264 (2021), https://doi.org/10.1016/j.seppur.2021.118353.

[43] K. El Hassani, H. Jabkhiro, D. Kalnina, B.H. Beakou, A. Anouar, Effect of drying step on layered double hydroxides properties: application in reactive dye intercalation, Appl. Clay Sci. 182 (2019) 105246, https://doi.org/10.1016/j.clay.2019.105246.

[44] I. Ogino, R. Tanaka, S. Kudo, S.R. Mukai, The impact of thermal activation conditions on physicochemical properties of nanosheet-derived Mg-Al mixed oxides, Microporous Mesoporous Mater. 263 (2018) 181–189, https://doi.org/10.1016/j.micromeso.2017.12.014.

[45] H. Ji, W. Wu, F. Li, X. Yu, J. Fu, L. Jia, Enhanced adsorption of bromate from aqueous solutions on ordered mesoporous Mg-Al layered double hydroxides (LDHs), J. Hazard Mater. 334 (2017) 212–222, https://doi.org/10.1016/j.jhazmat.2017.04.014.

[46] W. Yang, Y. Kim, P.K.T. Liu, M. Sahimi, T.T. Tsotsis, A study by in situ techniques of the thermal evolution of the structure of a Mg-Al-CO3 layered double hydroxide, Chem. Eng. Sci. 57 (2002) 2945–2953, https://doi.org/10.1016/S0009-2509(02)00185-9.

[47] R. Zăvoianu, R. Bîrjega, E. Angelescu, O.D. Pavel, Effect of hydration temperature on the reconstruction of Mg-Al-Y layered materials, Compt. Rendus Chem. 21 (2018) 318–326.

[48] J.Y. Lee, G.H. Gwak, H.M. Kim, T. Il Kim, G.J. Lee, J.M. Oh, Synthesis of hydrotalcite type layered double hydroxide with various Mg/Al ratio and surface charge under controlled reaction condition, Appl. Clay Sci. 134 (2016) 44–49, https://doi.org/10.1016/j.clay.2016.03.029.

[49] N. Jinapong, M. Suphantharika, P. Jamnong, Production of instant soymilk powders by ultrafiltration, spray drying and fluidized bed agglomeration, J. Food Eng. 84 (2008) 194–205, https://doi.org/10.1016/j.jfoodeng.2007.04.032.

[50] M.R.I. Shishir, W. Chen, Trends of spray drying: a critical review on drying of fruit and vegetable juices, Trends Food Sci. Technol. 65 (2017) 49–67, https://doi.org/10.1016/j.tifs.2017.05.006.

[51] P.D. Hede, P. Bach, A.D. Jensen, Two-fluid spray atomisation and pneumatic nozzles for fluid bed coating/agglomeration purposes: a review, Chem. Eng. Sci. 63 (2008) 3821–3842, https://doi.org/10.1016/j.ces.2008.04.014.

[52] R.V. Tonon, C. Brabet, M.D. Hubinger, Influence of process conditions on the physicochemical properties of açai (Euterpe oleraceae Mart.) powder produced by spray drying, J. Food Eng. 88 (2008) 411–418, https://doi.org/10.1016/j.jfoodeng.2008.02.029.

[53] J.J. Nijdam, T.A.G. Langrish, The effect of surface composition on the functional properties of milk powders, J. Food Eng. 77 (2006) 919–925, https://doi.org/10.1016/j.jfoodeng.2005.08.020.

[54] M.R.I. Shishir, F.S. Taip, N.A. Aziz, R.A. Talib, M.S. Hossain Sarker, Optimization of spray drying parameters for pink guava powder using RSM, Food Sci. Biotechnol. 25 (2016) 461–468, https://doi.org/10.1007/s10068-016-0064-0.

[55] G. Kaur, S.J. Couperthwaite, G.J. Millar, Acid mine drainage treatment using bayer precipitates obtained from seawater neutralization of bayer liquor, Glob. Challenges. 2 (2018) 17–22, https://doi.org/10.1002/gch2.201800061.

[56] V. Rives, Study of layered double hydroxides by thermal methods, in: Vicente Rives (Ed.), Layer. Double Hydroxides Present. Futur., first ed., Nova Science Publishers, Nova York, 2001, pp. 127–152, https://doi.org/10.1192/bjp.112.483.211-a.

[57] I. Melián-Cabrera, M. López Granados, J.L.G. Fierro, Thermal decomposition of a hydrotalcite-containing Cu-Zn-Al precursor: thermal methods combined with an in situ DRIFT study, Phys. Chem. Chem. Phys. 4 (2002) 3122–3127, https://doi.org/10.1039/b201996e.

[58] S. Kouva, J. Andersin, K. Honkala, J. Lehtonen, L. Lefferts, J. Kanervo, Water and carbon oxides on monoclinic zirconia: experimental and computational insights, Phys. Chem. Chem. Phys. 16 (2014) 20650–20664, https://doi.org/10.1039/c4cp02742f.

[59] S. Kouva, K. Honkala, L. Lefferts, J. Kanervo, Review: monoclinic zirconia, its surface sites and their interaction with carbon monoxide, Catal. Sci. Technol. 5 (2015) 3473–3490, https://doi.org/10.1039/c5cy00330j.

[60] E.F.S. Vieira, A.R. Cestari, R.A. Chagas, G.K.D.R. Cortes, Obtenção e caracterização de matriz apropriada para sistemas de liberação prolongada-estudos de liberação dos herbicidas atrazina e diuron, Quim. Nova 37 (2014) 398–403, https://doi.org/10.5935/0100-4042.20140074.

[61] L. Markov, V. Blaskov, D. Klissurski, S. Nikolov, The thermal decomposition mechanism of iron(III) hydroxide carbonate to α-Fe2O3, J. Mater. Sci. 25 (1990) 3096–3100, https://doi.org/10.1007/BF00587656.

[62] R.W. Stevens Jr., R.V. Siriwardane, J. Logan, In situ fourier transform infrared (FTIR) investigation of CO2 adsorption onto zeolite materials, Energy Fuel. 22 (2008) 3070–3079, https://doi.org/10.1021/ef800209a.

[63] L. Lv, J. He, M. Wei, D.G. Evans, X. Duan, Uptake of chloride ion from aqueous solution by calcined layered double hydroxides: equilibrium and kinetic studies, Water Res. 40 (2006) 735–743, https://doi.org/10.1016/j.watres.2005.11.043.